ELSEVIER

Journal of Fluids and Structures 20 (2005) 801–816

JOURNAL OF FLUIDS AND STRUCTURES

www.elsevier.com/locate/jfs

An experimental study of the nonlinear dynamics of cylindrical shells with clamped ends subjected to axial flow

K.N. Karagiozis, M.P. Païdoussis*, A.K. Misra, E. Grinevich

Department of Mechanical Engineering, McGill University, 817 Sherbrooke Street West, Montreal, Québec, Canada H3A 2K6

Received 15 October 2004; accepted 31 March 2005

Abstract

This paper presents experimental results on the nonlinear dynamics and stability characteristics of thin-walled clamped–clamped circular cylindrical shells in contact with flowing fluid. The experiments were conducted with three experimental set-ups: one for experiments with elastomer shells in annular air-flow, the second for elastomer shells with internal air-flow, and the last one for aluminium or plastic cylindrical shells with internal water-flow. In all cases the interaction between the shell and the fully developed flow gives rise to instabilities in the form of static or dynamic divergence at sufficiently high flow velocities. The aim of the experimental study was (i) to gather data on the critical flow velocity for instability and on the post-critical flow/displacement–amplitude relationship, and (ii) to undertake an analysis of the experimental results and to compare them qualitatively with theoretical predictions. The experimental results show a softening type nonlinear behaviour, with a large hysteresis in the velocity for the onset and cessation of divergence.

Keywords: Shells conveying fluid; Shells in annular flow; Nonlinear dynamics; Experimental bifurcation diagrams; Divergence; Coupled-mode flutter; Dynamic divergence

1. Introduction

Most of the research on fluid–structure interactions involving plates and shells focused on compressible and especially on supersonic flow, reflecting the great interest there is in the effect of high-speed flow on the outer-skin panels of aircraft, missiles and aerospace vehicles; see, e.g., Dowell's (1975) monograph. However, there are many other applications in which shells are subjected to *incompressible* or *subsonic flows*, which are also of great interest. Among them are: thin cylindrical shells used as thermal shields in nuclear reactors and heat shields in aircraft engines; shell structures in jet pumps, heat exchangers and storage tanks; and thin-walled piping for aerospace vehicles. Furthermore, in biomechanics, veins and pulmonary passages can be modelled as shells conveying fluid.

For a long time, it was believed that subsonic/incompressible flows were associated with loss of stability in the form of mild divergence—in contrast to the vigorous flutter and richer dynamics observed with supersonic flows. However, the work of Païdoussis and Denise (1972) has sparked new interest in the study of shells subjected to subsonic flows. Païdoussis and Denise, in addition to their experiments with cantilevered and clamped–clamped shells, also provided

*Corresponding author. Tel.: +1 514 398 6294.
E-mail address: mary.fiorilli@mcgill.ca (M.P. Païdoussis).

0889-9746/$ - see front matter © 2005 Elsevier Ltd. All rights reserved.
doi:10.1016/j.jfluidstructs.2005.03.007

the first analytical model for this system: a linear model, using Flügge's shell equations and assuming the flow to be inviscid. Additional work was conducted by Weaver and Unny (1973), Shayo and Ellen (1974), and many others. The effect of viscosity, which can be very important, was examined by Païdoussis et al. (1985), El Chebair et al. (1989) and Nguyen et al. (1994). For a detailed literature review, see Païdoussis (2003a).

The physical behaviour observed in experiments with shells conveying fluid, considering here only shells with clamped ends since this is the topic of this paper, is that at sufficiently high flow velocity the system develops flutter [see Païdoussis and Denise (1972)]. Linear theory, on the other hand, predicts that the system should lose stability by divergence, and then at higher flow by coupled-mode flutter. The interval between the two is generally small, especially if the fluid conveyed is air. Hence, it was reasoned that in the experiments of Païdoussis and Denise (1972) flutter was *entrained* by the divergence, and hence that was the reason why divergence by itself was not observed. In the case of external (annular) flow, however, divergence *was* observed, but not flutter, as reported by El Chebair et al. (1989)—though the maximum flow velocities available were probably insufficient to reach the critical flow for flutter.

Mindful of the controversy on the existence of post-divergence coupled-mode flutter in pipes conveying fluid, which was only resolved via nonlinear theory [see Païdoussis (1998, 2003b)], it is clear that its existence for the shell problem would have to be decided by nonlinear theory in this case also—thereby, hopefully, clarifying also the nonoccurrence of divergence in the internal flow experiments. The interesting questions raised in the work discussed above were partly responsible for providing the impetus for the nonlinear analysis of shells with supported ends, conveying, or immersed in, fluid. Amabili et al. (1999) have developed a nonlinear analytical model for shells with simply supported ends, using the Donnell nonlinear shallow shell equations and the Païdoussis and Denise linear inviscid fluid–structure interaction model. The most significant findings of this work are two: (a) the system loses stability by a strongly subcritical pitchfork bifurcation, meaning that divergence may occur at much lower flows than the linear threshold; (b) only static (stable or unstable) solutions are found to exist beyond the first bifurcation (i.e., no oscillatory solutions are predicted). Similar results have been obtained for external flow by Amabili et al. (2001).[1]

The foregoing provide the motivation for the experiments to be described: namely to investigate whether (a) and (b) above are true—for shells with *clamped ends*, for experimental convenience. The difference between clamped and simply supported ends is expected to affect the dynamics only quantitatively.

2. Apparatus

The three different set-ups involved in the experiments on thin circular cylindrical shells subjected to either annular or internal axial flow are described in this section. For the annular flow experiments, the cylindrical shell was positioned inside a concentric rigid tube, with air flowing in the annular space. For the experiments with internal flow, different types of cylindrical shells (elastomer, aluminium, plastic) were subjected to flow of either water or air. The different experimental apparatuses, along with the test procedures and instruments used for the measurement of flow and shell deformation, are discussed in the following subsections.

2.1. Annular flow apparatus

Fig. 1 shows the apparatus used in the annular flow experiments. In the upper part, above the surface of the "table", an elastomer shell is clamped at both ends and positioned coaxially within the outer rigid tubular cylinder.

This outer rigid tube, which provides the outer containment of the annular flow, is made of plexiglas and is mounted coaxially on the upper end of a wooden plenum chamber. A specially designed ring is mounted at the upper end of the plexiglas tubular cylinder to provide the clamped boundary condition for the elastomer shell. In these experiments, the annular gap was set at 6.4 mm.

The lower part of the apparatus consists of an axisymmetric plenum chamber with contracting ends. Inside the chamber, three flow screens and a honeycomb are mounted, ensuring proper enhanced mixing of the fluid and breakup of any existing large turbulent eddies. The well-mixed air–stream, prior to entering the annular region of the rubber shell, is further rendered uniform and straight by flowing through an annular region provided by a long solid cylinder with an ogival streamlined lower end. The annular passage, from its upstream end (i.e., from the ogival end of the upstream "solid cylinder", Fig. 1) to the upstream end of the shell, is approximately $50D_h$ long, where D_h is the

[1]It should be mentioned that the effect of fluid viscosity, not taken into account, could change the theoretical findings, e.g., resulting in coupled-mode flutter or even making the system *lose* stability by flutter—see, e.g., Païdoussis (2003a).

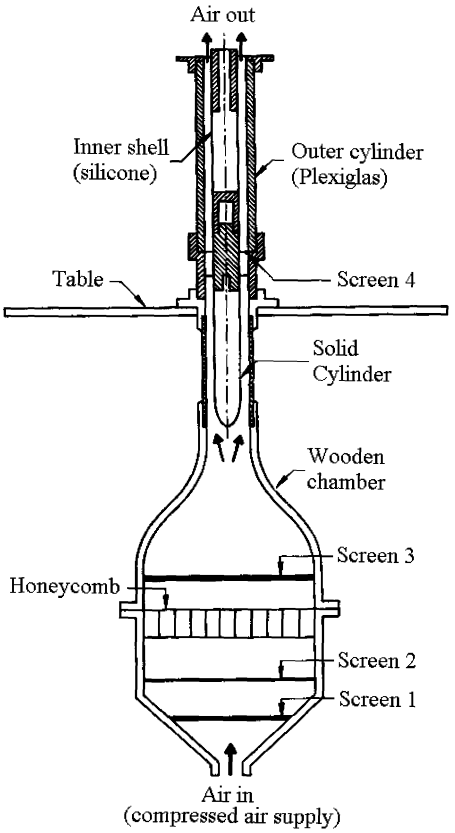

Fig. 1. Experimental apparatus for annular air-flow experiments with elastomer shells [after El Chebair et al., 1989].

hydraulic diameter; hence for the Reynolds numbers at instability, which are $Re_{D_h} \sim \mathcal{O}(10^4)$, where the subscript denotes that the Reynolds number is based on the hydraulic diameter, the flow should be turbulent and fully developed.

The air is supplied, at the bottom of the chamber, from a bank of compressors interconnected to a surge tank, providing air at about 690 kPa. Depending on the application, the pressure of the air entering the shell varied from 475 to 630 kPa.

Additional experiments were conducted to assess the effect of a steady transmural pressure difference, $\Delta P_{tm}(x) = P_{\text{ann}}(x) - P_{\text{inn}}$, where $P_{\text{ann}}(x)$ is the static pressure in the annulus at a specific point, e.g., at the downstream end of the shell ($x = L$), and P_{inn} is the static pressure of the quiescent inner fluid. Fig. 2(a) shows the arrangement in which $P_{\text{inn}} = P_a$, where P_a is the atmospheric pressure, so that $\Delta P_{tm}(x) = P_{\text{ann}}(x) - P_a$. In contrast, in Fig. 2(b), $P_{\text{inn}} = P_{\text{ann}}(L)$, and hence $\Delta P_{tm}(x) = P_{\text{ann}}(x) - P_{\text{ann}}(L)$. It should be noted that for the arrangement in both Fig. 2(a) and (b), $\Delta P_{tm}(x) = P_{\text{ann}}(x) - P_{\text{inn}} > 0$ over the whole length of the shell ($0 \leqslant x < L$); i.e., there is an inwards transmural pressurization. However, $\Delta P_{tm}(x)$ is larger in Fig. 2(a) than in Fig. 2(b). It is known that an inwards transmural pressure would tend to collapse (buckle) the shell, if it becomes sufficiently large. [It is worth noting that if $P_{\text{inn}} = P_{\text{ann}}(0)$, then $\Delta P_{tm}(x) < 0$ over the shell length; however, this arrangement was not tested in the present experiments.]

2.2. Internal flow apparatus

The internal flow experiments were conducted in two different experimental apparatuses. The first one was for the air-flow experiments with the elastomer shells, and the second for the water-flow experiments involving aluminium or plastic shells. A brief description of the two apparatuses is given in the following sub-subsections.

2.2.1. Internal air-flow experiments

Fig. 3 shows the apparatus used in the internal air-flow tests. The set-up is very similar to that for the annular flow experiments. The main difference is that, in this case, upstream of the shell, a convergent duct section is used to channel

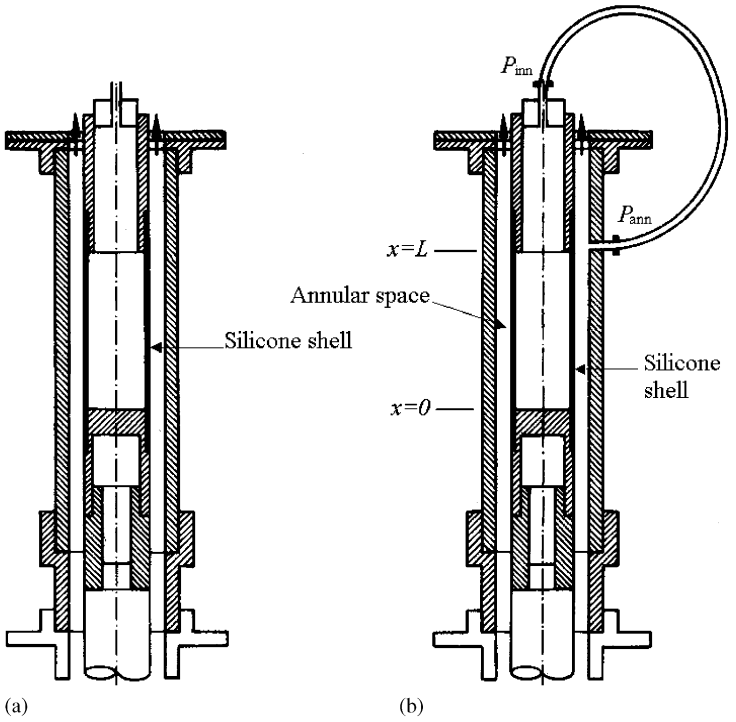

Fig. 2. Set-ups to study the pressurization effect in annular flow. (a) The inner static pressure is equal to the atmospheric pressure; (b) the inner static pressure in the shell (at $x = L$) is equal to the annular static pressure at the downstream end of the shell ($\Delta P_{tm}(x) = P_{ann}(x) - P_{inn} = P_{ann}(x) - P_{ann}(L)$). It is noted that the inwards pressurization in (a) is larger than in (b).

the air-flow from the upstream plenum to the shell. In these experiments, the annular gap, i.e., the distance between the external surface of the shell and the outer plexiglas cylinder (filled with quiescent air), remained constant and relatively large (38.5 mm) as compared to the shell radius (~25 mm).

Due to the flow limitations of the experimental set-up (maximum of 690 kPa in the air supply), it was impossible to observe instabilities for very short shells ($L/R = 2$ or smaller). Therefore, a second set of experiments was conducted including a solid aluminium cylindrical rod, with an ogival streamlined lower end, centrally positioned inside the clamped shell, as shown in Fig. 4(a). The radial gap between the elastomer shell and the aluminium rod was 12.5 mm.

All these experiments were conducted with the apparatus of Fig. 3 modified by a "pressurization opening", as shown in Fig. 4, such that $P_{ann} = P_{inn}(0)$. The transmural pressure $\Delta P_{tm}(x) = P_{ann} - P_{inn}(x) > 0$ for all $0 \leqslant x < L$; i.e., in this case, as in the annular flow experiments, the transmural pressure is positive inwards.

2.2.2. *Internal water-flow experiments*

The water-flow apparatus involves a modification of the water tunnel shown in Fig. 5. A centrifugal pump (Ingersol-Rand Centurion S), is used to circulate water driven by an SCR-controlled 40 hp motor (Beel Controls Ltd., speed regulation 0.1% at 95% of load change). The water tunnel provides average water velocities up to 6 m/s at the entrance of the plexiglas test-section, the inner diameter of which is 203 mm. The water static pressure in the water tunnel was kept at 41 ± 2 kPa, by an automatic feedback system. Upstream of the test-section, screens and a honeycomb are used to ensure proper mixing and uniformity of the flow. The water tunnel provides an acceptably flat mean flow velocity profile outside the boundary layer, as discussed by Gagnon (1989).

Inside the plexiglas test-section, a specially designed contraction, with the shell clamped at both ends, was installed as shown in Fig. 6. The design does not allow any flow to enter into the annular space between the shell and the cylindrical plexiglas outer wall of the test-section. The annular space is filled with quiescent water that can be pressurized, independently of the internal pressure in the tunnel, via an external pressurization line. In the notation adopted in this paper, we have $\Delta P_{tm}(x) = P_{ann} - P_{inn}(x) > 0$ for all $0 \leqslant x \leqslant L$, with P_{ann} not necessary related to any $P_{inn}(x)$.

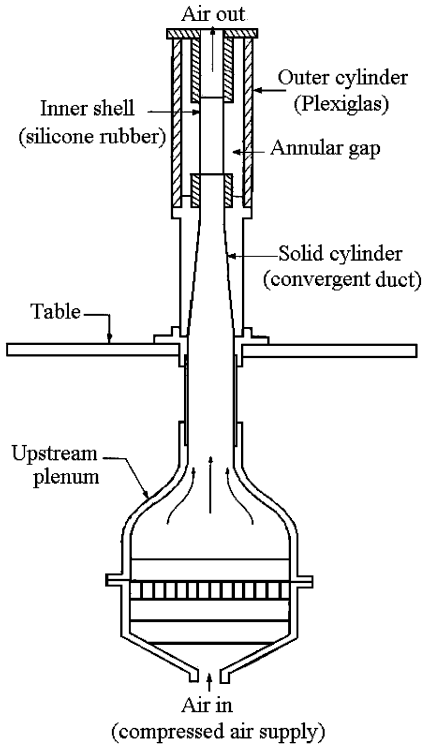

Fig. 3. Apparatus for internal air-flow experiments with elastomer shells.

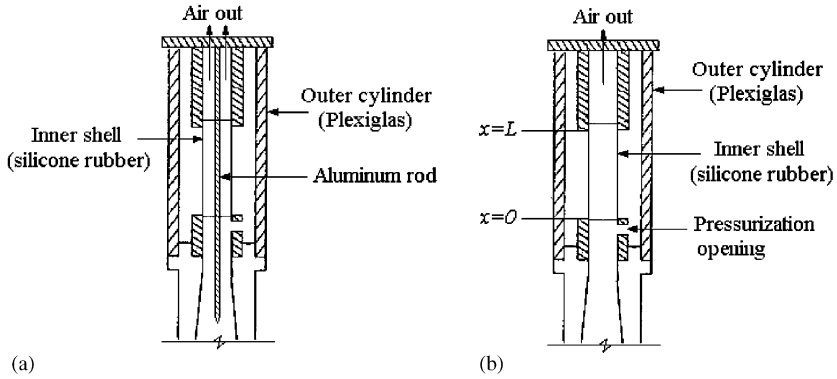

Fig. 4. Modifications to the internal air-flow apparatus of Fig. 3 for the experiments reported in this paper. In both (a) and (b) a pressurization opening generates an intramural pressure $\Delta P_{tm}(x) = P_{\text{ann}} - P_{\text{inn}}(x) = P_{\text{inn}}(0) - P_{\text{inn}}(x)$. In (a), additionally, an aluminium rod is installed centrally within the shell to allow attaining higher maximum flow velocities.

2.3. The shells used in the experiments

In the annular and internal air-flow experiments, only elastomer silicone-rubber shells were used. These shells were cast in a special mould. Liquid Silastic E-RTV (room temperature vulcanizing) was mixed with a catalyst and then injected into the specially designed mould. The material properties of these shells were determined from measurements conducted in house. Additional information on these shells (manufacturing, properties) may be found in Païdoussis (1998, Appendix D). The basic material properties for the particular silicone rubber shells used in the present work are given in Table 1.

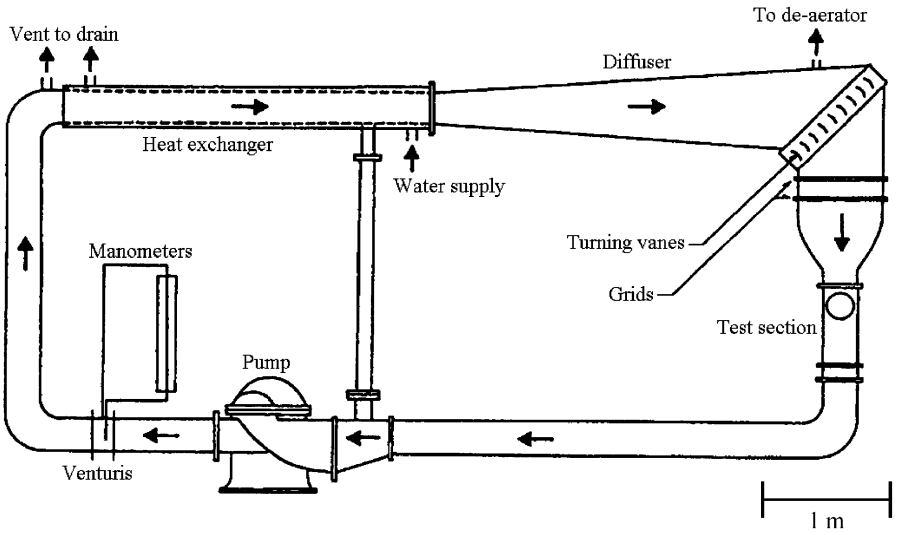

Fig. 5. The water tunnel used in the internal water-flow experiments [after Païdoussis, 2003a].

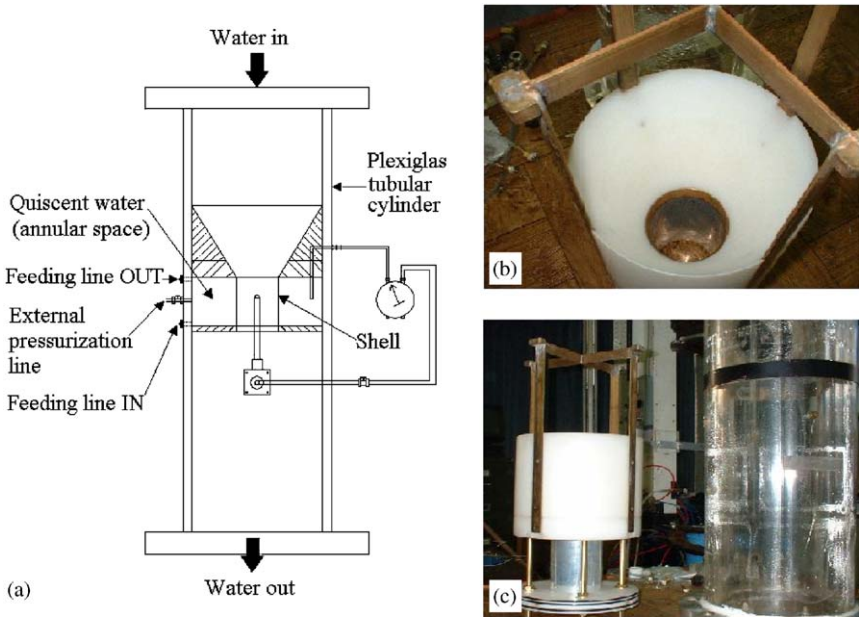

Fig. 6. View of the test-section of the water tunnel, with the apparatus for shells subjected to internal water-flow mounted in it: (a) schematic of the apparatus; (b) the plastic contraction, with the aluminium shell installed at its lower end; (c) the apparatus (left) before installation in the plexiglas test-section (right).

Table 1
Material properties for the shells used in the annular and internal flow experiments

Shell	E (N/m^2)	ρ_s (kg/m^3)	v
Silicone rubber	2.82×10^5	1.16×10^3	0.47
Aluminium	70×10^9	2.72×10^3	0.33
Plastic (PET)	2.3×10^9	0.8×10^3	0.4

E is Young's modulus, ρ_s the density of the material, v the Poisson ratio.

In the internal water-flow experiments, two different types of shell were used. In the first set of experiments, a thin shell made of aluminium 3104-H19 was employed. In the second set of experiments, a thin plastic shell made of Polyethylene Terephthalate (PET) was used. The material properties of the aluminium and plastic shells are also given in Table 1.

2.4. Instrumentation and measurements

In all annular and internal flow experiments, in both air and water tests, the main objective was: (i) to observe the dynamical behaviour of the system, (ii) to determine the threshold and nature of any instabilities that may arise, whether static or dynamic, and (iii) to record the maximum radial deformation of the shell with increasing and then decreasing flow, paying particular attention to the deformation amplitude versus flow-velocity relationship in the neighbourhood of instabilities. The instrumentation used to obtain the measurements for the flow velocity and shell amplitude is described in the following.

2.4.1. Flow velocity measurements

The flow velocity in the air-flow experiments was calculated from the flow rate measured by an orifice plate located upstream of the apparatus (Bean, 1971). Orifice plates of different sizes were used to accommodate a wide range of flow rates. The air temperature, inlet pressure and differential pressure across the orifice were measured and recorded.

The flow velocity in the internal water-flow experiments was calculated from the volumetric flow rate measured via one of the two Venturi-type insert nozzles (BIF model 131) mounted in parallel in the water tunnel. Mean flow velocity measurements were conducted to provide information on the velocity profile inside the shell (at mid-height). The measurements, along one diametral axis of the test-section, showed that the velocity profile is flat in the central region of the shell.

2.4.2. Shell amplitude measurements

In all experiments, instability in the form of divergence (buckling) developed abruptly, and hence it was necessary to capture its development carefully. For this, two analog noncontacting laser sensors and an analog video camera were used. The first laser sensor used (MATSUSHITA ANR 1282) has an output of 0–5 V, and a resolution of 4/13/40 μm. The frequency band was set to 'high' to capture possible vibrations of the shell during experiments at the high flows. An output controller (MATSUSHITA LM 10) was used to convert the laser signal to a voltage output. The second analog laser system (MICRO-EPSILON optoNCDT 1400-200) also has an output of 0–5 V. It has a static resolution of 40 μm and a dynamic resolution of 200 μm at 1 kHz. The controller model (DAYTRONIC 3263P) used with the second laser system offers the option of three frequency output ranges (5000, 10 000, and 20 000 Hz) to capture possible vibrations of the shell during the experiments.

Both laser systems were calibrated and the voltage outputs were converted to shell amplitude in millimeters. In the air-flow experiments only the first sensor was used, while for the water-flow experiments both sensors were employed.

In all cases, it was attempted to train the laser beam to the point of the maximum deformation of the shell. Fig. 7 shows the orientation of the laser beam to the vertical wall of the shell. The video camera was also set up to record the deformation of the shell on a VHS tape as the flow velocity was increased.

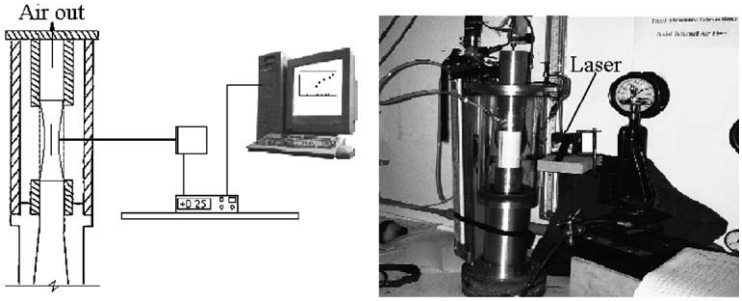

Fig. 7. Air-flow experiments and measurement equipment: (a) a schematic of the analog laser beam pointing at the point of maximum shell amplitude for an internal flow experiment; (b) photograph of the annular air-flow apparatus and the laser beam set-up.

2.5. Procedure

The same basic steps of operation were followed in all annular and internal flow experiments, as follows.

(i) The shell was mounted properly in the apparatus, such that there would be no initial pre-stress (e.g., axial compression) in the shell. All measuring instruments were positioned, and initial values were measured and recorded.
(ii) The flow was turned on, and the flow velocity was incremented in small steps. At each step, all readings from the instruments were recorded after steady state had been reached. This was continued until instability was reached. The flow was increased further to the maximum attainable, and then decreased to zero in small decrements.
(iii) Based on (ii), plots of shell amplitude versus flow velocity were obtained.

Additional steps in the procedure were introduced to accommodate different experimental objectives. In the annular flow experiments, in addition to the initial tests in which the internal pressure in the shell was equal to the atmospheric pressure (large ΔP_{tm}), a pressurization line (as in Fig. 2(b)) was used to equalize the static pressure of the annular flow at the downstream end of the shell to the static pressure of the internal shell area (smaller ΔP_{tm}), as discussed in Section 2.1. A similar approach was used to provide $\Delta P_{tm} > 0$ (inwards pressurization) in the internal air-flow experiments (see Fig. 4, and the discussion in Section 2.2.1). In the water-flow experiments the annular pressure was made to be higher than the internal one ($\Delta P_{tm} > 0$ again) via externally controlled pressurization of the annular fluid (Section 2.2.2). In this case, P_{ann} was adjusted at each flow velocity step to ensure that ΔP_{tm} remained constant, at the desired value.

3. Observations for clamped shells in annular flow

The dimensions of the shell used in these experiments are given in Table 2; L is the length, D the external diameter, and R the internal radius of the shell. In all cases, divergence was observed for high enough flow velocities, with the shell collapsing inwards.

A typical bifurcation diagram, illustrating the nonlinear behaviour of the shell with increasing and decreasing flow is shown in Fig. 8, in a case where $\Delta P_{tm}(x) = P_{\text{ann}}(x) - P_{\text{inn}} > 0$ with $P_{\text{inn}} = P_{\text{ann}}(L)$. It is seen that at small flow velocities the shell remained stable and essentially undeformed. Small static deformations developed as the flow velocity was increased, reaching 0.2 mm approximately at a flow velocity $U = 40\,\text{m/s}$; this is likely associated with the growth of initial imperfections in the shell. At $U = 40.4\,\text{m/s}$ the shell lost stability by divergence. The shell walls moved inwards, and a new stable static equilibrium was established with a radial deformation of 5 mm, corresponding to 3 times the shell thickness; this divergence was associated with a circumferential wavenumber (number of nodal diameters) of $n = 4$, as shown in inset of Fig. 8. This value of n is in agreement with previous experimental results and theoretical calculations (El Chebair et al., 1989).

The flow velocity was then decreased slowly, and more data-points were recorded, as shown in the figure. At $U = 35.8\,\text{m/s}$, the shell returned to its original circular shape of zero wall displacement. This flow-dependent hysteresis shows that the divergence instability is subcritical; i.e., the nonlinear behaviour is of the softening type. This subcritical behaviour of the shell has been confirmed by repeating the experiment a number of times.

3.1. Pressurization effect

The results presented in Fig. 8 were obtained with a moderate ΔP_{tm}, corresponding to $P_{\text{inn}} = P_{\text{ann}}(L)$, for the arrangement of Fig. 2(b). The experiment was repeated with a larger inwards pressurization, corresponding to $P_{\text{inn}} = P_a$, i.e., for the arrangement of Fig. 2(a). As seen in Table 3, and as expected, the additional inwards pressurization destabilizes the system; i.e., the critical flow velocity is lower. This had been observed previously by El

Table 2
Shell dimensions for the annular and internal air-flow tests

Shell system	Length, L (mm)	Diameter, D (mm)	Thickness, h (mm)	L/R
Annular air-flow	40–60	51.20	1.5	1.7–2.5
Internal air-flow	23.5–104.3	50.09	1.5	1.0–4.4

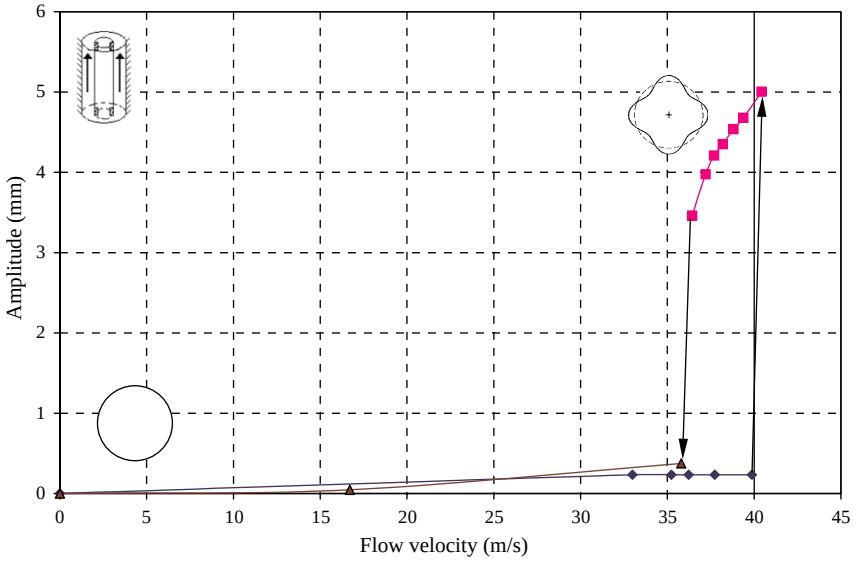

Fig. 8. The amplitude versus flow velocity diagram for an elastomer shell ($L/R = 1.7$) subjected to annular air-flow with moderate intramural pressure, $\Delta P_{tm}(x) = P_{\text{ann}}(x) - P_{\text{inn}}$.

Table 3
Pressurization effect for the air-rubber annular flow system ($L/R = 1.7$)

Pressurization	Instability	U_c (m/s)	U_R (m/s)	N	A (mm)	Loss of stability
$P_{\text{inn}} = P_{\text{ann}}(L)$	Divergence	40.4	35.8	4	5.00	Subcritical
$P_{\text{inn}} = P_a$	Divergence	19.8	18.1	4	1.77	Subcritical

U_c is the critical flow velocity for buckling, U_R the restabilization flow velocity, n the circumferential wavenumber, A the radial shell amplitude, and P_a the atmospheric pressure.

Chebair et al. (1989, Table 5), but the effect here is much more pronounced. The reason for this is that the shell used in these experiments is much shorter than those used by El Chebair et al. ($L/R = 6$). The lower end of the shell was positioned as in Fig. 2, but for a shorter shell the upper end of the shell is much further from the downstream end of the annulus; thus, the difference between $P_{\text{ann}}(L)$ and P_a is much larger, and the additional inwards pressurization in the arrangement of Fig. 2(a) vis-à-vis that of Fig. 2(b) is much more significant.

Fig. 9 shows some additional results obtained by changing the value of ΔP_{tm} in the course of the experiment. Initially, $\Delta P_{tm}(x) = P_{\text{ann}}(x) - P_{\text{ann}}(L)$, i.e., $P_{\text{inn}} = P_{\text{ann}}(L)$. When the flow velocity reached $U = 40.2\,\text{m/s}$, the shell lost stability by divergence with a circumferential wavenumber of $n = 4$ (point A in Fig. 9). The amplitude of the radial shell deformation was 3.55 mm, or 2.4 times the shell thickness. Once this first point of instability was reached, (ΔP_{tm}) was increased by removing the tube in Fig. 2(b), thus reverting to the arrangement of Fig. 2(a), leaving the inner fluid at a pressure equal to the atmospheric pressure. This resulted in an immediate increase of the shell amplitude from 3.55 to 5.80 mm (with $U = 40.2\,\text{m/s}$), or 3.9 times the shell thickness (point B in Fig. 9). This additional inwards intramural pressurization (2.7 kPa at $x = L$) therefore resulted in an amplitude increase of 63% (going from point A to point B with the same flow velocity). The circumferential wavenumber, however, remained the same. The flow was then slowly decreased to zero, and restabilization of the shell occurred at $U = 19.4\,\text{m/s}$ with the shell going back to its original circular cross-sectional shape, with a larger hysteresis than in Fig. 8 due to the higher value of ΔP_{tm} in this case.

3.2. L/R ratio effect

The effect of the length-to-radius ratio in the annular air-flow experiments is summarized in Table 4 for $P_{\text{inn}} = P_{\text{ann}}(L)$. It is shown that for $L/R = 2.5$ the shell lost stability by divergence at a critical flow velocity of about

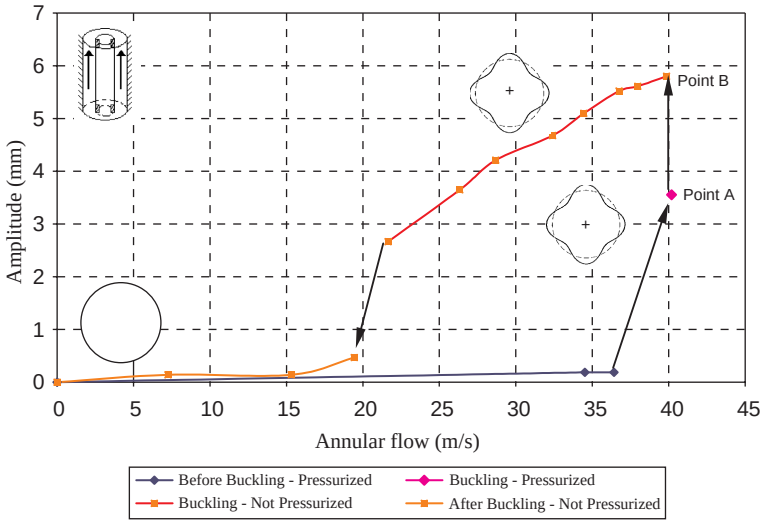

Fig. 9. The amplitude versus flow velocity diagram for an elastomer shell ($L/R = 1.7$) subjected to annular air-flow. Initially, $\Delta P_{tm}(x) = P_{\text{ann}}(x) - P_{\text{ann}}(L)$, i.e., $P_{\text{inn}} = P_{\text{ann}}(L)$, leading to buckling at point A. Then, $\Delta P_{tm}(x)$ was increased to $\Delta P_{tm}(x) = P_{\text{ann}}(x) - P_a$, $P_{\text{ann}}(L) - P_{\text{inn}} = 2.7\,\text{kPa}$, and the amplitude jumped to point B.

Table 4
Effect of L/R on the critical flow velocity and circumferential wavenumber in annular air-flow

L/R	U_c (m/s)	Circumferential wavenumber, n	Pressurization	Loss of stability
2.5	33.5	3	$P_{\text{inn}} = P_{\text{ann}}(L)$	Subcritical
1.7	40.5	4	$P_{\text{inn}} = P_{\text{ann}}(L)$	Subcritical

33.5 m/s with $n = 3$. For a $L/R = 1.7$ the shell lost stability by divergence at a higher flow velocity, $U = 40.5\,\text{m/s}$, and with a higher circumferential wavenumber, $n = 4$.

In both cases the shell exhibited a nonlinear subcritical behaviour (with a hysteresis in returning to the original stable condition). These results show a strong relationship between the L/R ratio and the critical flow velocity and circumferential wavenumber at divergence.

3.3. Concluding remarks for the annular flow experiments

It is concluded from all the experiments with annular flow that the shell loses stability by a strong subcritical divergence.

Experiments indicated that enhanced inwards intramural pressurization of the shell, i.e., larger inward-directed pressure difference across the shell wall, severely destabilizes the shell. This is not surprising, since it is clear that, if the pressurization were increased sufficiently, the shell would buckle, even with no flow.

Finally, it was found that as the length was reduced the circumferential wavenumber associated with divergence increased, which accords with previously found results; e.g., Païdoussis (2003a).

All these observations agree qualitatively with linear and nonlinear theory predictions (Païdoussis, 2003a; Amabili et al., 2001).

4. Observations for clamped shells with internal air-flow

In all internal air-flow cases the shell system lost stability by divergence leading to *dynamic* buckling. The mechanism of dynamic buckling is explained in Fig. 10: (i) the shell walls collapse inwards because of the divergence as in Fig. 10(b),

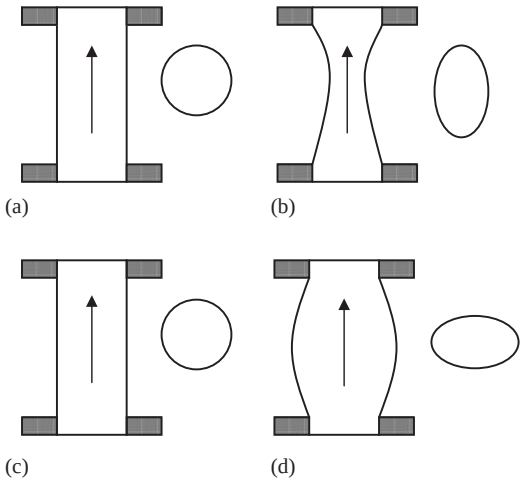

Fig. 10. The dynamic buckling sequence for internal air-flow: (a) the shell shape just before buckling; (b) the shell loses stability by large-amplitude buckling ($n = 2$), resulting in a pressure build-up upstream of the shell; (c) the pressure build-up forces the shell back to its circular shape and then (d) to its anti-phase buckled shape. The diagrams on the right depict the cross-section of the shell at the point of maximum deformation.

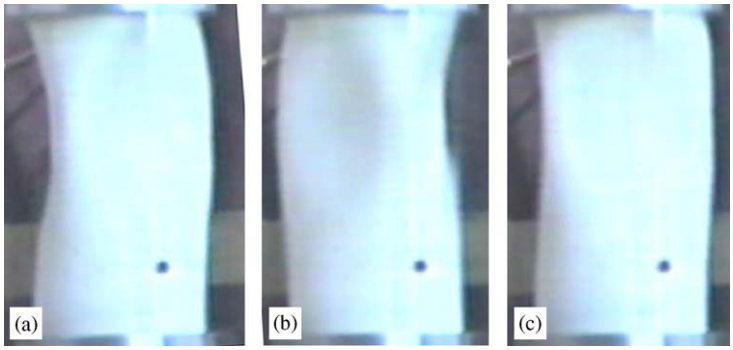

Fig. 11. The phenomenon of dynamic buckling for an elastomer shell with internal air-flow: (a) the buckled shell near its critical flow velocity (with shell amplitude of 6.0 mm and $n = 3$); (b) the pressure build-up causes the shell to open and then deform in its anti-phase buckled shape; (c) again the pressure build-up deforms the shell back to nearly the same shape as in (a); only nearly the same, because the time interval between (a) and (c) is not exactly one period of the oscillation.

with sufficient amplitude, because of the high flexibility of the shell, for the flow to be considerably constricted; (ii) the resultant build-up of upstream pressure forces the shell to reopen as in Fig. 10(c); (iii) because of the forces leading to divergence and inertia, the reopened shell does not remain in its circular cross-sectional shape, but it goes to an anti-phase buckled shape, as in Fig. 10(d); (iv) this is repeated dynamically, so that the observed alternation of buckled shapes produces a "breathing" oscillation, indistinguishable from flutter.

Fig. 11 shows in a series of photographs the dynamic buckling phenomenon, as observed in one of the experiments for a shell with $L/R = 4.4$. The shell dimensions for this experiment are given in Table 2. In this experiment the aluminium rod was used inside the shell; see Fig. 4(a).

In the first photograph, Fig. 11(a), the shell has lost stability by divergence with an amplitude of 6 mm and $n = 3$. At this flow, the gap between the shell and the aluminium rod at the point of maximum displacement had been reduced by 50%, with an attendant reduction in flow area. Therefore, the large build up or air pressure causes the shell to open up and to buckle in the anti-phase shape shown in Fig. 11(b). This phenomenon is repeated again, and the shell returns to nearly the previous deformed shape as shown in Fig. 11(c) [nearly but not quite, because Figs. 11(a) and (c) are not quite one period apart]. This continued as long as the flow velocity remained in the neighbourhood of the critical velocity

value. The shell deformation in the sequence of photographs shown in Fig. 11 occurs in fractions of a second; the frequency of oscillation in this experiment was of the order of 12 Hz.

Additional tests indicated that a kind of circumferential travelling wave might exist during the violent vibration of the shell.

4.1. Effect of L/R ratio

In subsequent experiments, the effect of smaller L/R on the critical flow velocity was studied. Table 5 gives the results for four shells, with the annular pressure equal to the inner pressure at $x = 0$ (upstream end of the shell), for different L/R ratios. In all cases the shell lost stability by divergence. It is evident that shorter shells require a higher flow to become unstable. Reducing the length of the shell results also in an increase in the circumferential wavenumber.

4.2. Effect of flow perturbations

Because of the violent nature of the dynamic buckling phenomenon, it was difficult to obtain exact values for the shell amplitude at buckling and almost impossible to obtain exact values for the restabilization velocity. Furthermore, the vibration was so violent that it sometimes destroyed the shell. Hence, a gentler approach was used to obtain some useful data-points. The air-flow was kept as low as possible, and strong flow perturbations were generated downstream of the shell. It was found that the disturbance-induced instability occurred at a lower critical flow velocity than that occurring spontaneously. Because the flow was smaller, the shell buckled and vibrated less violently, thus allowing the collection of some useful information.

For example, in one such case for $L/R \simeq 4$, buckling occurred at $U = 22.6\,\mathrm{m/s}$ with $n = 3$. With no perturbation, under the same set-up conditions, buckling occurred at $U = 28.4\,\mathrm{m/s}$. The fact that divergence could be induced at smaller flow velocities than the critical suggests that, in this case also, the divergence is strongly subcritical.

5. Observations with clamped shells with internal water flow

In the experiments with internal water flow the stability of two different shells was investigated, one made of aluminium and the other of PET-C93 plastic. The dimensions of both shells are listed in Table 6. In the water-flow experiments, both shells lost stability by divergence subcritically and experienced a nonlinear hysteresis before restabilization.

Table 5
Effect of L/R to the critical flow velocity in internal air-flow experiments with the elastomer shell with $P_{\mathrm{ann}} = P_{\mathrm{inn}}(0)$

L/R	U_c (m/s)	n	Reynolds number
4	28.39	3	8.9×10^4
3	31.85	3	9.9×10^4
2	36.85	4	1.2×10^5
1	40.97	4	6.8×10^4

In the case of $L/R = 1$, the inner aluminium rod was used as in Fig. 4(a), and hence the Reynolds number is based on the hydraulic diameter, Re_{D_h}.

Table 6
Shell dimensions for the internal water-flow tests

Shell system	Length (mm)	Diameter (mm)	Thickness (mm)	Length/radius, L/R
Aluminium	122.5	82.25	0.137	2.98
Plastic (PET)	100.1	83.6	0.300	2.41

5.1. Aluminium shell results

Because of the limitations of the water tunnel (the maximum flow velocity in the plexiglas test-section is 6 m/s) and the high flexural rigidity of the aluminium shell, a substantial transmural pressure ΔP_{tm} (acting inwards) was necessary during the experiments in order to obtain buckling. This pressure difference was always set well below the critical pressure of static buckling of the shell. A representative set of results from these experiments is shown in Fig. 12. The transmural pressure, in this case $\Delta P_{tm}(L/2) = P_{\text{ann}} - P_{\text{inn}}(L/2) = 5.7\,\text{kPa}$, and it was kept at this value as the flow velocity was varied. The flow velocity was incremented until instability occurred. The shell lost stability by divergence at a critical flow velocity of $U = 16.4\,\text{m/s}$ with a circumferential wavenumber of $n = 6$. The radial deformation of the shell at the first point of buckling was 2.45 mm, about 18 times the shell thickness. When slowly decreasing the flow velocity, the shell amplitude was also decreased until the original circular cross-sectional shape was restored at $U = 9.3\,\text{m/s}$.

In contrast to the elastomer shells, the flexural rigidity here is sufficiently large to result in relatively small amplitude at divergence (compared to the shell radius), hence incurring no appreciable constriction of the flow area. This is believed to be the reason for the nonoccurrence of dynamic divergence.

Once more, the subcritical and softening nonlinear response of the shell is clearly illustrated in Fig. 12 (compare the critical velocity of $U_c = 16.4\,\text{m/s}$ to the restabilization velocity of $U_R = 9.3\,\text{m/s}$).

A representative visual example of the shell divergence for the aluminium shell is given in Fig. 13, showing the shell just before and right after divergence.

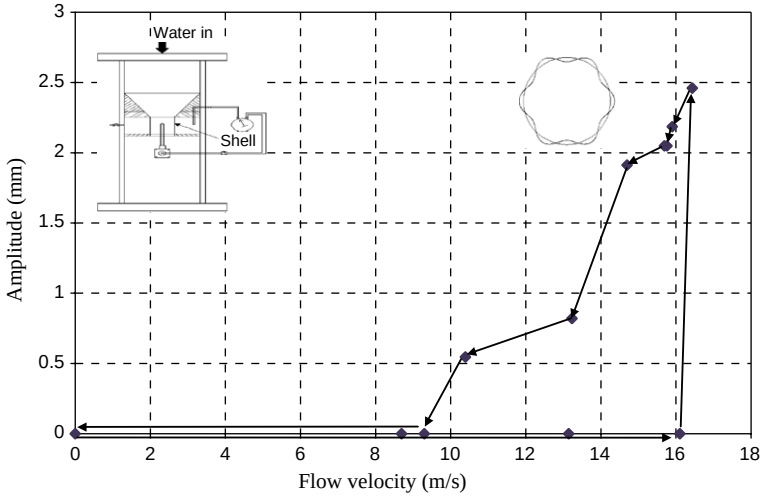

Fig. 12. The amplitude versus flow velocity diagram for an aluminium shell ($L/R = 2.98$) subjected to internal water-flow and inwards intramural pressurization; $\Delta P_{tm}(x) = P_{\text{ann}} - P_{\text{inn}}(x) > 0$ and $P_{\text{ann}} - P_{\text{inn}}(L/2) = 5.7\,\text{kPa}$.

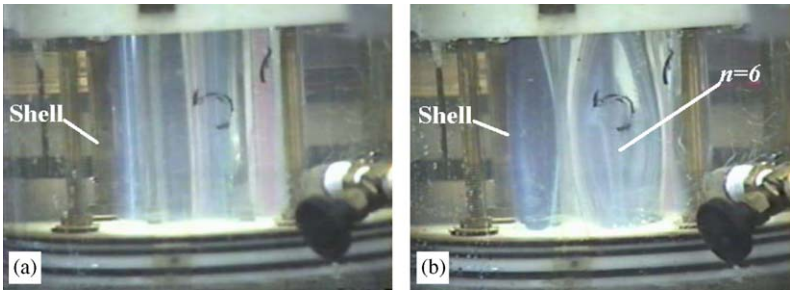

Fig. 13. The aluminium shell in internal water-flow: (a) before instability and (b) when divergence has occurred. (Note: these photographs are not from the same experiment as that of Fig. 12.)

Additional experiments were conducted for a range of differential pressures, and data-points for the critical flow velocity and shell displacement were recorded. In all cases the shell exhibited a softening type of nonlinear response. A set of these results is compiled in Table 7.

5.2. PET shell results

Additional experiments investigated the stability of a PET plastic shell with internal water flow. The plastic shell offers the advantage of a lower Young's modulus compared to the aluminium shell, as shown in Table 1. In these experiments, the differential pressure ($\Delta P_{tm}(L/2) = P_{\text{ann}} - P_{\text{inn}}(L/2)$) was generally lower than in the aluminium shell experiments. In the experiments to be presented, ΔP_{tm} was set at 5 kPa.

A typical set of results is shown in Fig. 14 as a plot of shell amplitude versus flow velocity. The flow was increased until buckling occurred at $U = 15.1$ m/s with $n = 6$. The shell amplitude at the first point of buckling was 3.1 mm, or 10 times the shell thickness. The flow was then reduced in steps, and the varying shell amplitude was recorded, as shown in the figure. At $U = 14.3$ m/s the shell regained its original cross-sectional circular shape. The results show the subcritical nature of the divergence instability and the nonlinear hysteresis as the flow was reduced.

Subsequent experiments, with higher ΔP_{tm}, have shown that U_c for buckling decreases, as expected. In all cases the loss of stability was subcritical. Table 7(b) shows the effect of ΔP_{tm} on the critical flow velocity and maximum shell amplitude at divergence.

Table 7
Aluminium and PET shells in internal water flow

Shell name	$\Delta P_{tm}(L/2)$(kPa)	U_c(m/s)	Shell amplitude (mm)
(a) *Aluminium shells*			
S3	4.5	16.3	2.7
S2	6.8	14.7	3.6
S1	9.6	10.6	3.8
(b) *PET shells*			
P1	6.2	14.0	2.7
P2	5.8	14.6	2.3

The effect of differential pressure, $\Delta P_{tm}(L/2) = P_{\text{ann}} - P_{\text{inn}}(L/2)$, on the critical flow velocity $U_c$and shell amplitude ($n = 6$).

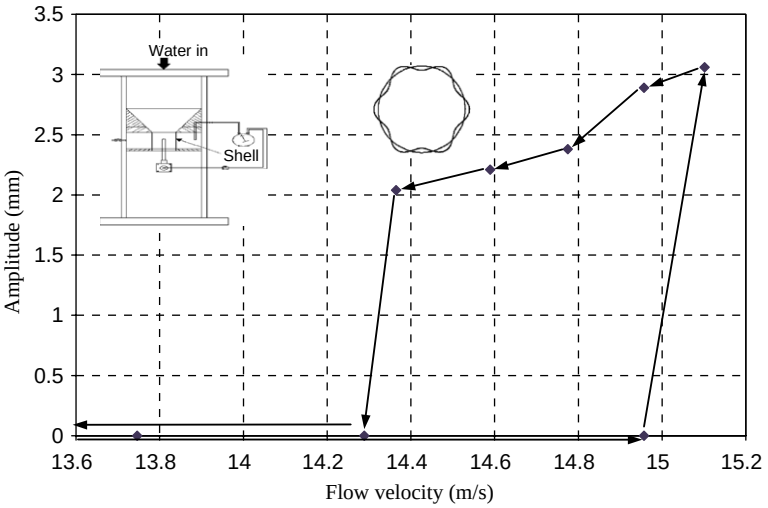

Fig. 14. The amplitude versus flow velocity diagram for a PET plastic shell ($L/R = 2.41$) subjected to internal water-flow, with intramural pressurization; $\Delta P_{tm}(x) = P_{\text{ann}} - P_{\text{inn}}(x) > 0$ and $P_{\text{ann}} - P_{\text{inn}}(L/2) = 5$ kPa.

6. Conclusions

Analysis of the experimental data shows that thin circular cylindrical shells conveying fluid lose stability by divergence. For shells that are not too flexible (e.g., the aluminium and PET plastic shells) with internal water-flow, and also for the annular flow experiments, a clear static divergence was observed. In the internal flow experiments with elastomer shells, however, the large-amplitude-related constriction at divergence resulted in a dynamic buckling phenomenon.

By decreasing the flow velocity, after buckling, it was observed that the shell returns to its original circular cross-sectional shape at a much smaller flow velocity than that necessary to cause buckling with increasing flow. This is clearly a subcritical nonlinear behaviour (softening-type nonlinear response), observed for both internal and external (annular) flow.

The critical flow velocity (velocity value at buckling) and circumferential wavenumber for divergence are both a function of the physical properties and geometry of the shell and of the transmural mean pressure, i.e., the differential pressure between the internal and external fluids; e.g., increasing the inwards transmural pressure, divergence occurs earlier as a combined effect of fluid–structure interaction and pressure difference. There is a clear relationship between the L/R ratio and the critical flow velocity U_c, with larger L/R leading to lower U_c and lower values of n (the circumferential wavenumber). Similarly, flow perturbations induce instabilities at much lower flow values.

Another important observation is that, other than the dynamic buckling discussed above (which could be mistaken for flutter), no true flutter was ever observed. It is important to mention, however, that additional interesting instabilities might exist at higher flow velocities, which could not be observed (if indeed they do exist) due to the limitations of the air and water apparatuses.

A new theoretical study has been undertaken for shells with clamped ends with either internal or external flow, for direct quantitative comparison with these experiments. In this theory the nonlinear Donnell shallow shell theory is used in conjuction with the Païdoussis and Denise linear model for the fluid flow. Analytical results have been obtained with a seven degree-of-freedom expansion for the radial shell deformation, using driven and companion asymmetric modes, as well as axisymmetric modes. The resulting equations are discretized in a Galerkin type solution, taking advantage of the spatially periodic form of the flow perturbations (as embedded in the travelling-wave formulation of Païdoussis and Denise). Bifurcation diagrams (amplitude versus flow velocity) are in excellent qualitative and quite reasonable quantitative agreement with the annular and internal flow experiments reported here. These results will be presented in a subsequent paper.

Also, some calculations with empty and water-filled shells subjected to forced vibration were found to be in good agreement with those obtained via another model for clamped shells and with experiment (Karagiozis et al., 2005).

Acknowledgments

The authors would like to thank NSERC of Canada and FCAR of Québec for their financial support. We would like to thank Dr M. Amabili for his help and advice during the experiments and Mr R. Burt of Ball Packaging Corporation for kindly supplying the aluminium shells.

References

Amabili, M., Pellicano, P., Païdoussis, M.P., 1999. Nonlinear dynamics and stability of circular cylindrical shells containing flowing fluid. Part I: Stability. Journal of Sound and Vibration 225, 655–699 see also Parts II–IV, published in 1999 and 2000.

Amabili, M., Pellicano, F., Païdoussis, M.P., 2001. Nonlinear stability of circular cylindrical shells in annular and unbounded axial flow. Journal of Applied Mechanics 68, 827–834.

Bean, H.S., 1971. Fluid Meters—their Theory and Applications, 6th ed. ASME, New York.

Dowell, E.H., 1975. Aeroelasticity of Plates and Shells. Noordhoff International, Leyden.

El Chebair, A., Païdoussis, M.P., Misra, A.K., 1989. Experimental study of annular-flow-induced instabilities of cylindrical shells. Journal of Fluid and Structures 3, 349–364.

Gagnon, J.O., 1989. Fluid coupling and response characteristics of cylinder clusters in axial flow. Ph.D. Thesis, McGill University, Montreal, Canada.

Karagiozis, K.N., Amabili, M., Païdoussis, M.P., Misra, A.K., 2005. Nonlinear vibrations of clamped circular cylindrical shells. In: Proceedings Third M.I.T. Conference on Computational Fluid and Solid Mechanics. Cambridge, MA, USA, p. 180.

Nguyen, V.B., Païdoussis, M.P., Misra, A.K., 1994. A CFD-based model for the study of the stability of cantilevered coaxial cylindrical shells conveying viscous fluid. Journal of Sound and Vibration 176, 105–125.

Païdoussis, M.P., 1998. Fluid–Structure Interaction: Slender Structures and Axial Flow, vol. 1. Academic Press, London.
Païdoussis, M.P., 2003a. Fluid Structure Interaction: Slender Structures and Axial Flow, vol. 2. Elsevier Academic Press, London chapter 7.
Païdoussis, M.P., 2003b. Some quandaries and paradoxes in fluid–structure interactions with axial flow. In: Proceedings IUTAM Symposium on Fluid–Structure Interaction. Kluwer, Dordrecht, New Brunswick, NJ, USA, pp. 247–266.
Païdoussis, M.P., Denise, J.P., 1972. Flutter of thin cylindrical shells conveying fluid. Journal of Sound and Vibration 20, 9–26.
Païdoussis, M.P., Misra, A.K., Chan, S.P., 1985. Dynamics and stability of coaxial cylindrical shells conveying viscous fluid. Journal of Applied Mechanics 52, 389–396.
Shayo, L.K., Ellen, C.H., 1974. The stability of finite length circular cross-section pipes conveying inviscid fluid. Journal of Sound and Vibration 37, 535–545.
Weaver, D.S., Unny, T.E., 1973. On the dynamic stability of fluid-conveying pipes. Journal of Applied Mechanics 40, 48–52.